Bull Volcanol (1997) 58:539–556

ORIGINAL PAPER

A. Takada

Cyclic flank-vent and central-vent eruption patterns

Received: 18 March 1996 / Accepted: 14 January 1997

Abstract Many basaltic and andesitic polygenetic volcanoes have cyclic eruptive activity that alternates between a phase dominated by flank eruptions and a phase dominated by eruptions from a central vent. This paper proposes the use of time-series diagrams of eruption sites on each polygenetic volcano and intrusion distances of dikes to evaluate volcano growth, to qualitatively reconstruct the stress history within the volcano, and to predict the next eruption site. In these diagrams the position of an eruption site is represented by the distance from the center of the volcano and the clockwise azimuth from north. Time-series diagrams of Mauna Loa, Kilauea, Kliuchevskoi, Etna, Sakurajima, Fuji, Izu-Oshima, and Hekla volcanoes indicate that fissure eruption sites of these volcanoes migrated toward the center of the volcano linearly, radially, or spirally with damped oscillation, occasionally forming a hierarchy in convergence-related features. At Krafla, terminations of dikes also migrated toward the center of the volcano with time. Eruption sites of Piton de la Fournaise did not converge but oscillated around the center. After the convergence of eruption sites with time, the central eruption phase is started. The intrusion sequence of dikes is modeled, applying crack interaction theory. Variation in convergence patterns is governed by the regional stress and the magma supply. Under the condition that a balance between regional extension and magma supply is maintained, the central vent convergence time during the flank eruption phase is 1–10 years, whereas the flank vent recurrence time during the central eruption phase is greater than 100 years owing to an inferred decrease in magma supply. Under the condition that magma supply prevails over regional extension, the central vent convergence time increases, whereas the flank vent recurrence time decreases owing to inferred stress relaxation. Earthquakes of $M \geq 6$ near a volcano during the flank eruption phase extend the central vent convergence time. Earthquakes during the central eruption phase promote recurrence of flank eruptions. Asymmetric distribution of eruption sites around the flanks of a volcano can be caused by local stress sources such as an adjacent volcano.

Key words Fissure eruption · Dike · Flank eruption · Summit eruption · Central eruption · Crack interactions · Cyclic eruptive behavior

Editorial responsibility: W. Hildreth

Akira Takada
Department of Environmental Geology, Geological Survey of Japan, 1-1–3 Higashi, Tsukuba, Ibaraki, 305 Japan
Fax: + +81 298 54 3533
e-mail: takada@gsj.go.jp

Introduction

Many basaltic and andesitic polygenetic volcanoes exhibit cyclic activity consisting of flank eruptions and central eruptions. A polygenetic volcano may bring its magma plumbing system under a form of "self-control," i.e., a dike intrusion induces local compressive stress that impedes subsequent nearby intrusion prior to stress relaxation (Takada 1994a). Extension of this idea suggests that dikes may be intruded at progressively decreasing distances from the center of the volcano under conditions of constant magma supply and regional stress. If so, migration patterns of fissure eruptions or dike intrusion sites may provide a window into the stress history of a volcano under the self-imposed control of its own magma plumbing system. Lipman (1980a, b) and Khrenov et al. (1991) reported the uprift migration of eruptive fissure sites within the southwest rift zone of Mauna Loa, Hawaii, and at Kliuchevskoi, Kamchatka, respectively. However, the longer–term general pattern of vent migration remains unknown. Considerable data have nevertheless been recorded on the locations and ages of fissure eruptions at volcanoes throughout the world. Compiling these data and making derivative time-series diagrams of eruption sites (intrusion distances of dikes) can be an important means of evaluating volcano growth, of qualitatively inferring

the stress history within the volcano, and of predicting the next eruption site.

This paper proposes the use of time-series diagrams for fissure eruption sites, to infer a general migration pattern of eruption sites for selected volcanoes in the world and to evaluate the growth pattern of each volcano. A new model of the intrusion sequence of dikes beneath a polygenetic volcano is advanced, based on crack interaction theory (Takada 1994a, b). Factors governing variations of the migration patterns of eruption sites are discussed using the output-stress diagram of Takada (1994c).

Time-series diagram of eruption sites

The position of an eruption site of a polygenetic volcano is represented by polar co-ordinates as shown in Fig. 1a. For evaluation, two types of time-series diagrams of eruption sites are needed (Fig. 1b). One is a diagram showing the distance from the center (the summit, the central vent, or the caldera) to the farthest eruption site of one continuous eruptive episode (r–t diagram). In order to express the asymmetric distribution of eruptive fissure swarms such as rift zones, the flank of the volcano is divided into two regions, e.g., the northern flank and the southern flank. The subdivisions of the flank depend on the overall eruptive fissure pattern of the volcano. If the eruptive episode is also accompanied with flank eruptions on the opposite flank and a central eruption, the farthest eruption site on each flank and a central eruption site are plotted simultaneously on the diagram. The second diagram required is one showing the clockwise azimuth from a north reference direction (θ-t diagram).

Some fissure eruptions on the flank of a volcano may result from the fact that portions of a dike reach the surface along the path of down-rift dike intrusion. Thus, a time-series diagram of intrusion distance of dikes can be useful to evaluate the growth of a polygenetic volcano. The intrusion distance of a dike is defined as the horizontal distance from the center of a polygenetic volcano to the termination of a dike. The intrusion distance is inferred from dike-induced normal faulting (e.g., Koide and Bhattacharji 1975; Rubin and Pollard 1988) and/or from the down-rift propagation of seismic activity (e.g., Brandsdottir and Einarsson 1979). Such geophysical records of recent intrusive events are available only for Kilauea Volcano (Hawaii) and Krafla Volcano (Iceland). For lack of intrusive data on the other volcanoes considered, this paper mainly reports migration patterns of historically reported eruptive sites, for which time-series diagrams can readily be constructed.

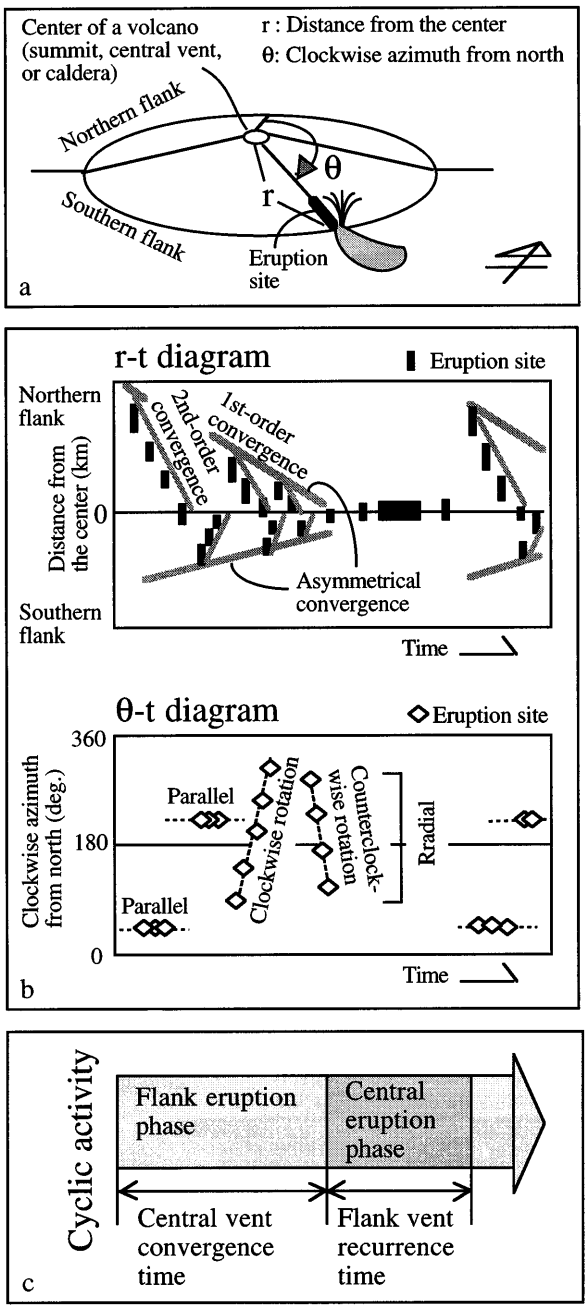

Fig. 1a Parameters representing the position of an eruption site. The flank of a volcano is divided into two regions, e.g., the northern flank and the southern one. **b** Two types of time-series diagram for eruption sites, representing the distance of eruption sites from the center (r–t diagram) and the clockwise azimuth from the north (θ–t diagram), respectively. **c** Schematic cyclic activity consisting of flank eruption and central eruption phases

Convergence patterns of eruption sites

Many polygenetic volcanoes have cyclic eruptive activity that alternates between a phase dominated by flank eruptions (flank eruption phase) and a phase dominated by eruptions from a central vent (central eruption phase; Fig. 1c). Flank eruptions may be accompanied by central eruptions. For example, if central eruptions without flank eruptions represent more than 70% of the total eruptions during a period, the period is defined as the central eruption phase. Many intermittent

eruptions or continuous eruptions within a year are counted as one eruption. In other words, the flux of magma supply toward a central vent is much larger than that toward the flank of a volcano during the central eruption phase. Volcanoes which do not clearly exhibit cyclic eruptive activity are discussed at the end of the paper.

Fundamental parameters on r–t diagrams are the central vent convergence time, the flank vent recurrence time, and the migration rate of eruption sites toward the center, and are listed in Table 1. The migration rate is defined as the distance of the farthest downrift eruptive fissure from the volcano's center divided by the central vent convergence time. Figure 2 shows a schematic summary of cyclic patterns from ten volcanoes during the past 2000 years, each of which are subsequently reported in detail in Figs. 3–11. The period evaluated depends, of course, on the historical records from each volcano. The flank eruption phase continues for periods of 10–1000 years (central vent convergence time); the central eruption phase continues for periods of 100–1000 years (flank vent recurrence time) (Figs. 1b, 2; Table 1). During the flank eruption phase, eruption sites migrate toward the center of the volcano (uprift migrations of fissure eruption sites). After the convergence of eruption sites, the central eruption phase starts. During this phase, continuous eruptions (the formation of a lava lake or a long-lived vent; e.g., Kilauea and Sakurajima volcanoes) or intermittent eruptions (e.g., Kliuchevskoi, Fuji, and Izu-Oshima volcanoes) occur. Fissure eruption sites on Piton de la Fournaise Volcano, however, did not converge but oscillated mainly inside the horseshoe-shaped caldera.

Some volcanoes show very complicated convergence patterns. A hierarchy in convergence-related features may be detectable in r–t diagrams as shown in Fig. 1b. Fissure eruption sites may converge with damped oscillation. This paper tries to define them temporarily as the first-order and/or the second-order convergences, respectively. Volcanoes developing parallel eruptive

Table 1 Parameters used in evaluating volcano growth

Volcano	Horizontal dimension (km)	Duration recorded (years)	Central vent convergence time (years)	Flank vent recurrence time (years)	Migration rate (km/years)
(1) Mauna Loa, Hawaii					
SWRZ (18th century-1994)	45	~ 200	~ 100	?	0.5
(2) Kilauea, Hawaii					
ERZ (18th century-1994)	60	~ 200	< 50	?	?
(3) Kliuchevskoi, Kamchatka					
(1697–1994)	22	262	62	> 243	0.4
(4) Etna, Sicily					
(15th century BC-1994)	20	~ 3500	~1000	~ 100	0.02
(5) Sakurajima, Japan					
(764–1914)	5	1150	1015	> 135	0.005
(1914–1994)	5	80	42	> 35	0.1
(6) Fuji, Japan					
(5000 years BP)	15	~ 5000	~1000	~1000	0.02
(7) Izu-Oshima, Japan					
(5th century-1994)	10	1500	~ 500	~ 500	0.02
(8) Hekla, Iceland					
(1554–1845)	7	290	290	~ 100	0.02
(1913–1994)	19	81	> 81	?	0.2
(9) Krafla, Iceland					
(1724–1994)	65	270	10	246	6.5
(10) Piton de la					
Fournaise, Réunion					
(1708–1994)	15	286	∞	0	–
(11) Eldgjá –					
Lakagigar, Iceland[a]	35	~ 1000	~ 1	849	–
(934–1994)					
(12) Veidivötn, Iceland[a]					
(~150–1994)	40	~ 2000	~ 1?	665	–
(13) Great Rift, Idaho[a]					
(15000 years BP)	85	~15000	~ 1?	~2000	–

[a] Monogenetic volcanoes. In the case of monogenetic volcanoes, the convergence time and the recurrence time are defined as the average duration of one eruption, and the average eruption interval in the monogenetic volcano field, respectively

References: (1) and (2) Lipman (1980a, b), Macdonald et al. (1983), Holcomb (1987), Peterson and Moore (1987), Lockwood and Lipman (1987), and Lockwood et al. (1987); (3) Khrenov et al. (1991), Ozerov et al. (1994), Simkin and Siebert (1994); (4) Chester et al. (1985), Romano (1991), Simkin and Siebert (1994); (5) Kobayashi and Ishihara (1988), Kobayashi (1988); (6) Tsuya (1968), Miyaji (1988), Uesugi (1993); (7) Nakamura (1964), Isshiki (1984), Sakaguchi et al. (1988); (8) Thorarinsson (1967), Thorarinsson and Sigvaldason (1972), Gronvold et al. (1983), Gudmondsson et al. (1992); (9) Tryggvason (1984); (10) Ludden (1977), Stieltjes et al. (1986), Lénat and Bachélery (1988), Lénat et al. (1989), Stieltjes and Moutou (1989), Simkin and Siebert (1994); (11) Thordarson and Self (1993); (12) Larsen (1984); (13) Kuntz et al. (1986)

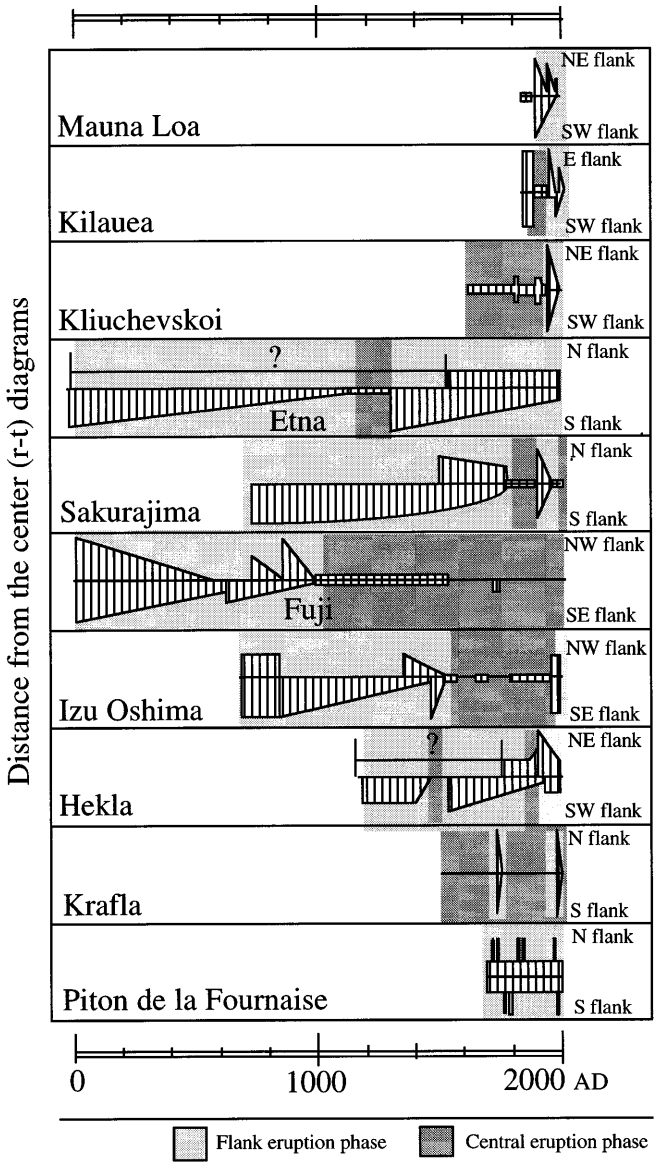

Fig. 2 Cyclic activity of volcanoes with convergence of eruption sites during the period evaluated. For Krafla Volcano, intrusion distance is used. The period evaluated depends on historical records of each volcano. *Striped polygon* represents space (distance from center of the volcano)–time distribution of eruption sites schematically. During the period and on the flank with a *question mark,* adequate data on site and age of eruption are not available

fissures show that activity alternates between rift zones a few times during a first-order convergence (θ-t diagram in Fig. 1b). Fissure eruption sites of some volcanoes converge asymmetrically on the two flank regions (asymmetric convergence; Figs. 1b, 2). Near or just after the convergence, some fissure eruption sites diverge with a long-distance intrusion that is very rapid (divergence of eruption sites). Then, fissure eruption sites begin to converge again abruptly, during one or a few eruptive events (abrupt convergence patterns within 150 years in the diagrams of Sakurajima and Izu-Oshima volcanoes in Fig. 2).

The θ-t diagrams of volcanoes developing radial eruptive fissures (dikes) indicate that their azimuths rotate occasionally with the convergence (Fig. 1b). In this case the azimuthal reference angle of an eruption site increases or decreases systematically with time in the diagrams.

Evaluation of volcano growth

Mauna Loa and Kilauea

Mauna Loa and Kilauea volcanoes, located on the island of Hawaii, are large basaltic shield volcanoes, whose radiating rift zones are arranged subparallel (Fig. 3a).

Eruption sites along the southwest rift zone of Mauna Loa have migrated toward the summit caldera since 1868 (Fig. 3b; Lipman 1980a, b). The convergence patterns along the southwest rift zone and northeast rift zone of Mauna Loa are asymmetric. Rift zone activity was shifting between two rift zones: The northeast rift zone was active during the periods of 1852, 1855, 1880–1881, 1899, 1935, and 1942; the southwest rift zone was active during the periods of 1868, 1887, 1907, 1919, 1926, and 1950 (Peterson and Moore 1987; Lockwood and Lipman 1987). In 1975 and 1984, fissure eruptions occurred in or around the summit caldera (Lockwood et al. 1987), which are regarded as those near the convergence point. The central vent convergence time of Mauna Loa along the southwest rift zone is around 100+ years, if the last flank eruption phase started in 1868. The 1500- to 2000-years cycle reported by Lockwood (1995), which is far longer than the central vent convergence time, may include repetitions of the shorter cycle proposed in this paper.

The convergence system of Kilauea is more complicated than that of Mauna Loa, owing to the existence of many intrusion episodes as well as to the formation of a long-lived vent along the rift zone. Eruption sites along the east rift zone of Kilauea (Macdonald et al. 1983; Holcomb 1987) may have crudely migrated toward Mauna Ulu during the period 1955 to 1969, and toward Pu'u O'o during the period 1977–1983 (Fig. 3c). Assuming that such migrations mean vague convergences, the central vent convergence time may be less than 50 years. Before the 1955 eruption, central eruptions have been dominant for more than 150 years since the 1790 caldera formation; flank eruptions also occurred more than 30 km from the summit caldera in 1823, 1840, and 1884(?) (Macdonald et al. 1983; Peterson and Moore 1987). At least the first half of the twentieth century may be the central eruption phase (Fig. 3c).

Kliuchevskoi (Klyuchevskoy)

Kliuchevskoi Volcano is the most active basaltic volcano on the Kamchatka peninsula. During the period 1697–1931 since discovery of the volcano, central erup-

tions had been dominant, making up 90% of the 39 recorded eruptions (Khrenov et al. 1991; Simkin and Siebert 1994). Convergence of eruption sites commenced during the flank fissure eruption of 1932. Eruption sites migrated toward the summit with oscillation and rotation (Fig. 4b, c). Khrenov et al. (1991) reported that flank eruption sites migrated toward the summit with time. Almost all flank eruptions occurred on the northeastern and the southeastern flanks (in the range of 0–180°; Fig. 4c). Volcanic activity during the period of 1932–1993 contains 47% flank eruptions and 53% central eruptions without flank eruptions (Simkin and Siebert 1994). A large summit eruption occurred in 1994 (Ozerov et al. 1994). Presently, the volcano appears to be at the beginning of a central eruption phase. If the period of 1697–1931 is regarded as the central eruption phase, the flank vent recurrence time of Kliuchevskoi is more than 234 years (Table 1).

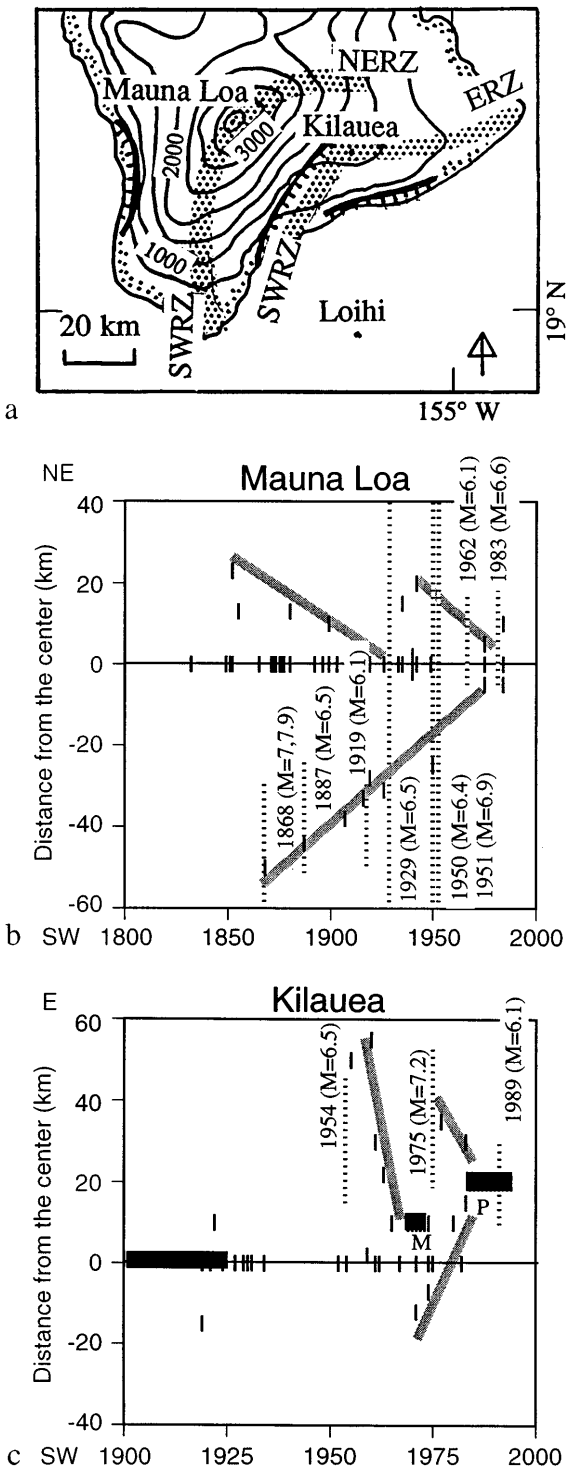

Fig. 3 **a** Locality map of Mauna Loa and Kilauea volcanoes, and **b, c** their r–t diagrams. Horizontal axis of the time-series diagram = years. At Mauna Loa positive values of distance from center represent sites along or around the northeast rift zone (*NERZ*); negative values represent sites along the southwest rift zone (*SWRZ*). The 1943 and 1859 eruptions on the north flank, far from the rift zones, are omitted. At Kilauea, positive values of distance from center represent sites along the east rift zone (*ERZ*); negative values represent sites along the southwest rift zone (*SWRZ*). *Bar* the farthest eruption site of each episode; *thick stippled line* trend of convergence as an interpretation; *thick horizontal bar* continuous eruption; *M* Mauna Ulu; *P* Pu'u O'o. *Vertical dotted line* from top to bottom = M ≥ 6 earthquake adjacent to the volcanoes; *vertical dotted line* part of the way = occurrence of M ≥ 6 earthquake along or near the rift zones. Data compiled from Lipman (1980a, b), Macdonald et al. (1983), Holcomb (1987), Peterson and Moore (1987), Lockwood and Lipman (1987), Lockwood et al. (1987), Wyss and Koyanagi (1992), and Dvorak (1994)

Etna

Etna Volcano, located on the island of Sicily, developed radial eruptive fissures that feature two prominent rift zones. Historical accounts of Etna's volcanism have been recorded since 1500 B. C. (Fig. 5a, b; Chester et al. 1985). The older the period of an eruption, of course, the larger the possibility that the events may not have been accurately recorded. However, eruptive events far from Etna's summit were recorded more frequently than those near the summit. There are enough events available for the construction of approximate time-series diagrams using historical records from the Roman age.

Volcanic activity during the period 1200–1990 contains 44% flank eruptions and 56% central eruptions without flank eruptions (Simkin and Siebert 1994). Figure 5b shows a hierarchy in convergence-related features during the period. Central vent convergence time of the first-order is 1000–1300 years; that of the second-order is 50–200 years. According to Chester et al. (1985), central eruptions were dominant during the period of 1169–1284(?), 1447–1536, and 1723–1755. Volcanic activity at Etna was either non-existent or was not recorded during the period 350–140 B. C. No information is available during the period 253–812 A. D. Eruption sites converged asymmetrically; sites on the northern flank are restricted to within 10 km from the summit (see dashed line in Fig. 5a and b), whereas those on the southern flank reach out 21 km. Eruptive fissure

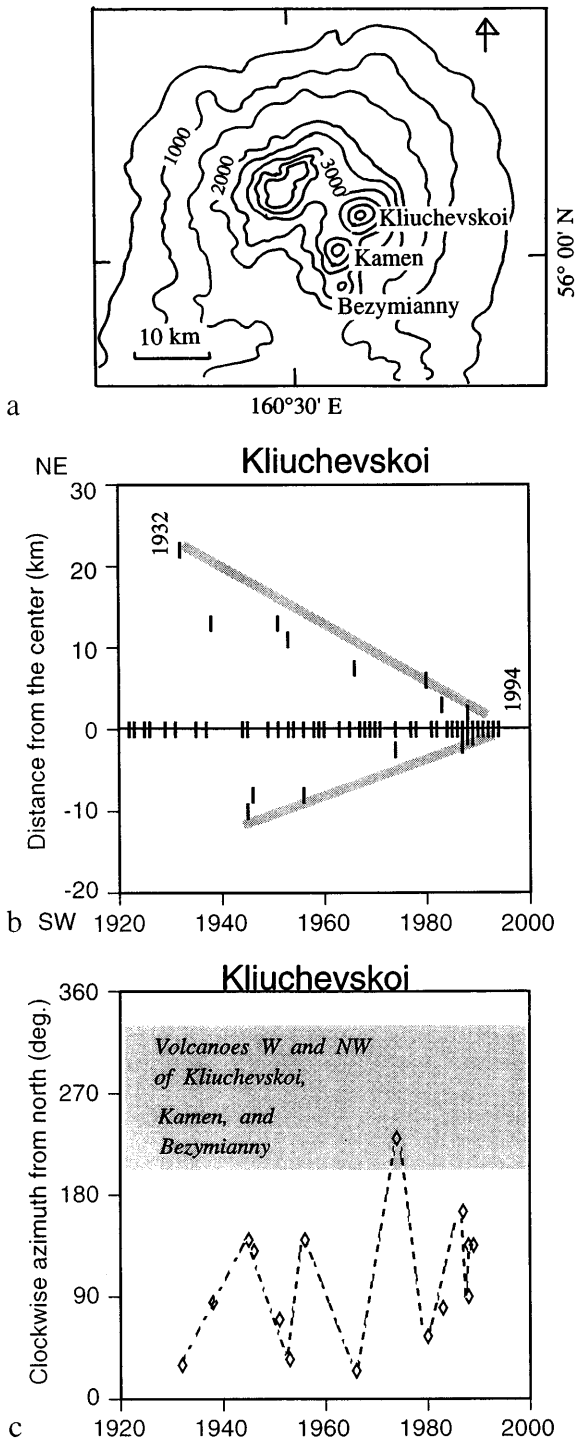

Fig. 4 **a** Locality map of Kliuchevskoi Volcano and **b, c** its r–t and θ-t diagrams. Positive values of distance from center are on the northeastern flank; negative values are on the southwestern flank. *Dashed line* the trend of rotation or oscillation; *stippled region* azimuths of adjacent volcanoes. Other explanations are the same as in Fig. 3. Data compiled from Khrenov et al. (1991), Ozerov et al. (1994), and Simkin and Siebert (1994)

patterns tend to become more radial near the convergence point. Azimuths of fissure trends do not concentrate but spread around the periods of 1600–1650, 1800–1850, and 1900–1990 (Fig. 5c). Eruptive activity representative of the first-order convergence that began in 1381 has approached to within 5 km of the summit.

Sakurajima

Sakurajima Volcano, Kyushu, Japan, composed mainly of andesite, is located on the southern side of Aira caldera, which formed 22000 years ago (Kobayashi 1988). The volcano is composed of two overlapping cones: Kitadake, the older, and Minamidake, the younger (Kobayashi 1988). Sakurajima Volcano developed radial eruptive fissures. With a decrease in the interval of fissure eruptions, the migration rate increases (Fig. 6a; Table 1). Weak central eruptions during the seventeenth to eighteenth centuries may be evidence for activity near the second-order convergence point. The 1779 eruption occurred near the volcano's center. In the great 1914 eruption, the eruption sites rapidly diverged toward the east and west. Following the 1914 activity, fissure eruption sites converged at least until 1955 (Fig. 6b). Central eruptions have been continuing since 1955. The flank vent recurrence time estimated from the period after the 1779 eruption is 135 years (Table 1). However, it is difficult to estimate how long the central eruption phase will continue.

Azimuths of eruptive fissures rotated counterclockwise (see dashed lines in Fig. 6c). During the 1779 eruption, the eruption site on the northern flank did not rotate regularly (counterclockwise from 35 to 30°; short dashed line in Fig. 6c). During the 1914 eruption, the two eruption sites rotated through large angles, skipping the region of Kitadake (counterclockwise from 30 to 285° and from 195 to 105°; short and long dashed lines in Fig. 6c, respectively).

Fuji

Fuji Volcano, central Japan, is a large basaltic stratocone. Fuji developed sets of subparallel to radial eruptive fissures. The flank eruption phase and the central eruption phase have reciprocally cycled three times over a period of 11000 years (Miyaji 1988). According to tephrochronological studies with ^{14}C dating (e.g., Miyaji 1988; Uesugi 1993), the central eruption phase occurred during the periods of 8000–4500 years BP and 3000–2000 years BP. During the central eruption phase, a few flank eruptions occurred. Available data after 5000 years BP are plotted in Fig. 7b. Eruptions of the last flank eruption phase are dated more exactly than the others. During the first-order convergence of this phase, the second-order convergence may have been repeated a few times. Near the convergence point around 800–1000 A. D., eruptive fissures tended to be-

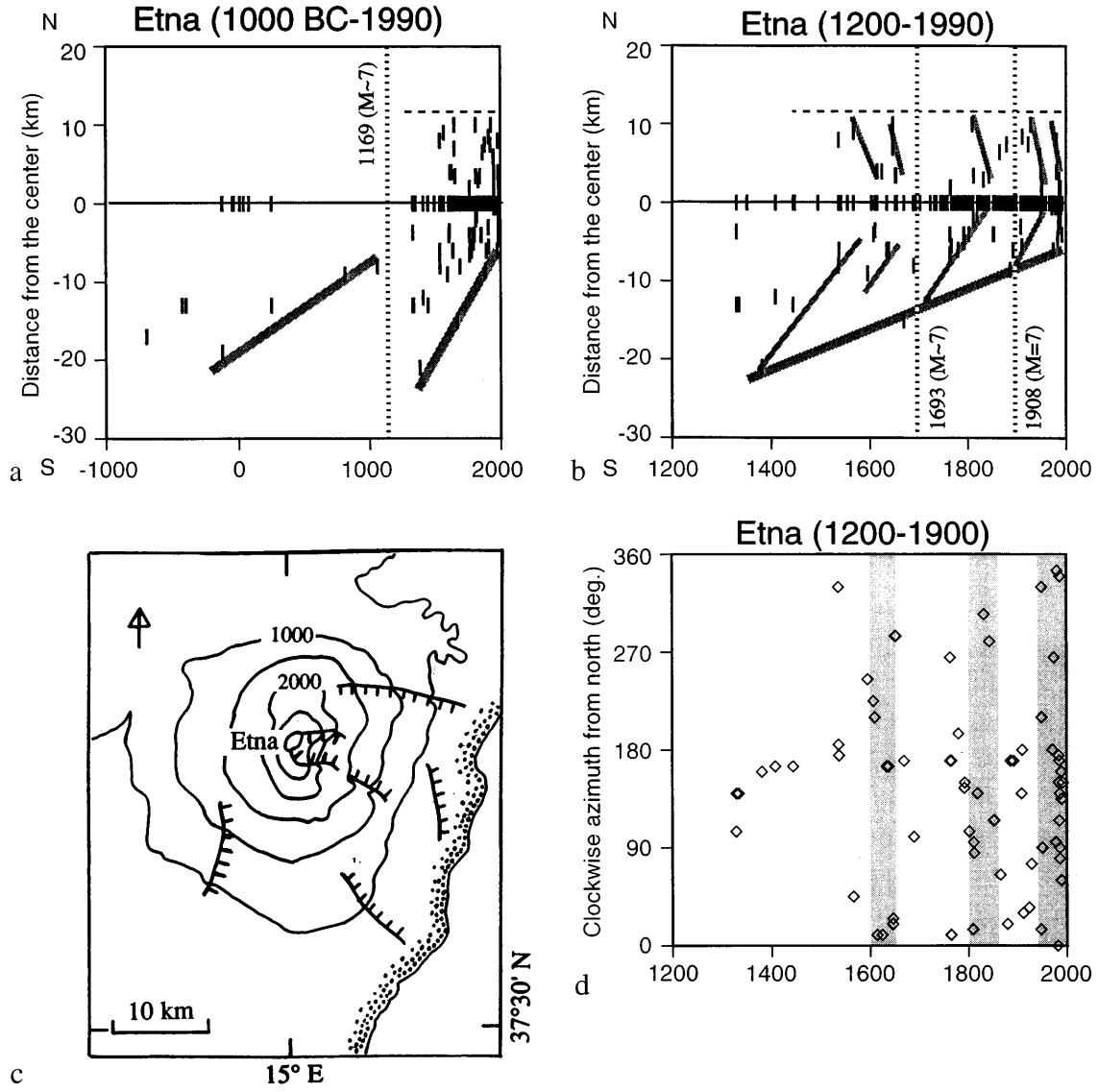

Fig. 5 **a, b, d** The r–t and θ–t diagrams of Etna Volcano, and **c** its locality map. Positive values of distance from center are on the northern flank; negative values are on the southern flank. *Thick stippled line* trend of interpreted first-order convergence; *thin stippled line* trend of interpreted second-order convergence. *Horizontal dashed line* represents the northern limit of fissure eruption sites. *Stippled region* in **d** period during which radial fissure eruptions are dominant. *Vertical dotted lines* large earthquakes beneath Sicily. Other explanations are the same as in Fig. 3. Data compiled from Chester et al. (1985), Romano (1991), Westaway (1992), and Simkin and Siebert (1994)

come radial (Fig. 7c). The central eruption phase started again around 1000 A. D. Since then, only the 1707 eruption has occurred as far as 4 km from the summit.

Izu-Oshima

Izu-Oshima Volcano, located just east of the Izu peninsula, Japan, is a basaltic volcano that developed parallel eruptive fissures. Historical eruptions were reported by Nakamura (1964) and Isshiki (1984). Around the fifth to seventh centuries, two calderas collapsed. On the southeastern flank, eruptive fissure sites began to migrate toward the center during the ninth century (Fig. 8b). The 1338 eruption occurred near the center. After the convergence on the southeastern flank, the eruptive fissure in 1421 diverged southeastward very rapidly. If an eruption inside the caldera is defined as a central eruption, the period of 1552–1974 is equivalent to a central eruption phase. The flank vent recurrence time is estimated to be approximately 500 years (Table 1). Furthermore, volcanic activity has been confined to Miharayama crater (a long-lived vent) from the 1777 eruption up to the 1986 eruption. The 1986 eruption was accompanied by eruptive fissures outside the caldera (e.g., Sakaguchi et al. 1988). Thus, the central eruption phase may have ended. Eruptive fissures developed on the northwestern and southeastern flanks during historic eruptions are asymmetric in distribution

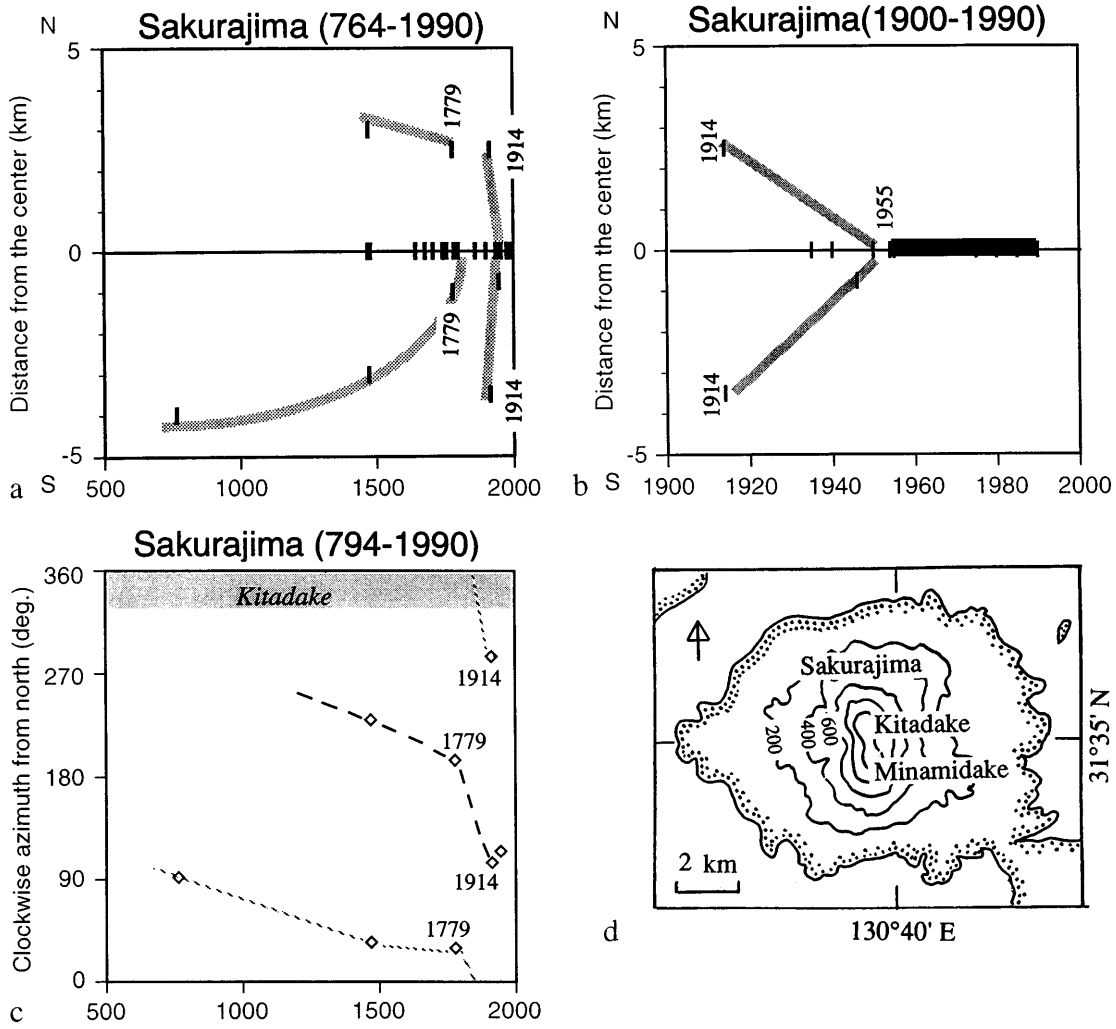

Fig. 6 The r–t and θ–t diagrams of **a–c** Sakurajima Volcano, and **d** its locality map. Positive values of distance from center are on the northern flank; negative values are on the southern flank. *Long and short dashed lines* in **c** trends of counterclockwise rotation. *Stippled region* in **c** azimuth of Kitadake. Other explanations are the same as Fig. 3. Data compiled from Kobayashi (1988) and Kobayashi and Ishihara (1988)

(Fig. 8b). Eruption sites on the northern flank were restricted to within 3 km of the center.

Hekla

Hekla Volcano is located on the western margin of the Eastern Volcanic zone, Iceland (Fig. 9a; Einarsson 1991; Gudmundsson et al. 1992). Near the volcano, the Eastern Volcanic zone connects with the South Iceland Seismic zone (SISZ). Volcanic activity has been recorded since the twelfth century (Thorarinsson 1967; Thorarinsson and Sigvaldason 1972). Fissure eruptions occurred in the region around Hekla Volcano, which was described as the "Hekla region" by Thorarinsson and Sigvaldason (1972), as well as on the flank of the volcano. All the fissures, including the Hekla region, are plotted in Fig. 9b and c. Eruption sites migrated toward the summit during the periods of 1554–1845 on the southwestern flank, and 1913–1991 on the northeastern flank. Fissure eruptions have occurred near the summit during the past 10 years. Eruption sites have closely approached the convergence point. Eruptive fissures tend to be radial near the convergence point (Fig. 9c).

Krafla

Krafla is located in the portion of Northern Volcanic zone, Iceland, that has developed en-echelon-arranged rift zones (Fig. 10a; Einarsson 1991). The 1975–1984 episode started after a repose interval of 246 years since the 1724–1729 episode (Tryggvason 1984). During the former episode, eruption sites were restricted to the region inside the Krafla caldera on the southern flank and within 11 km of the caldera center on the northern flank (Fig. 10b). However, terminations of dike intrusions migrated with some oscillations toward the caldera center. The region of intrusion was estimated

based on crustal deformation studies (Tryggvason 1984). Seismic evidence also supports dike intrusions (Bransdottir and Einarsson 1979). Second-order convergences have also been detected. The convergence pattern is asymmetric. The rift zone on the northern flank extends farther from the caldera than that on the southern flank. The volcano presently appears to have entered into a central eruption phase. The flank vent recurrence time is estimated to be approximately 250 years (Table 1).

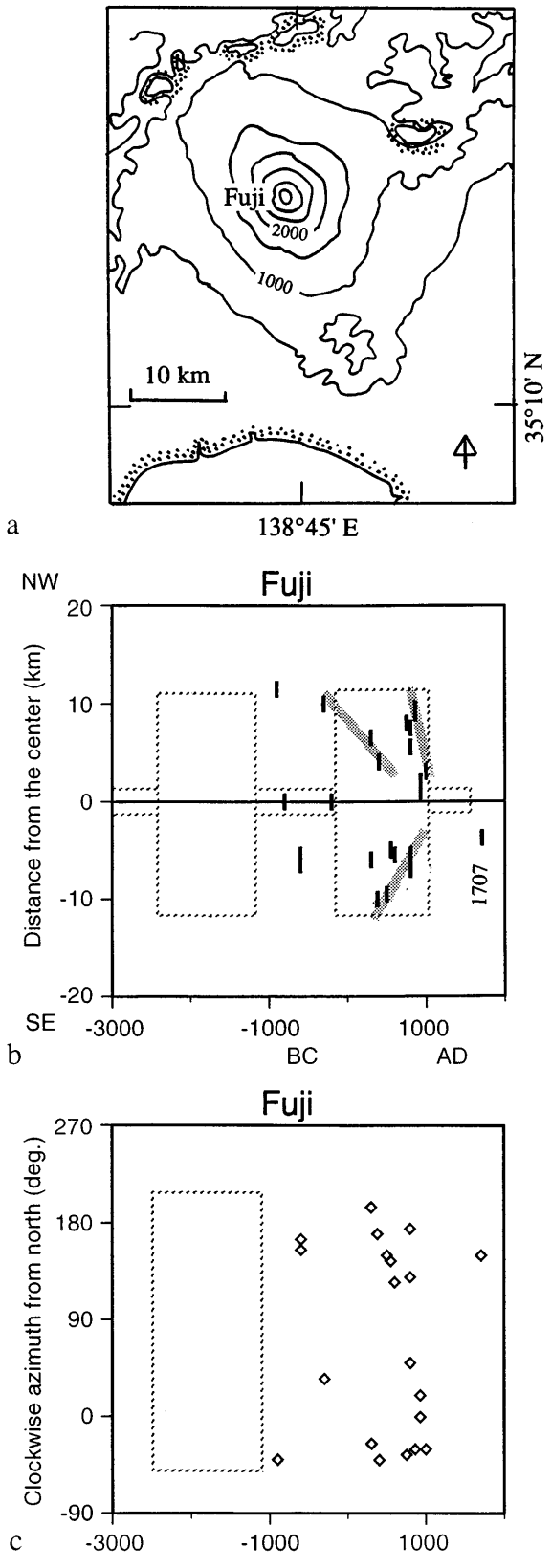

Piton de la Fournaise

Piton de la Fournaise is a basaltic shield volcano on Réunion Island in the Indian Ocean. It developed radial eruptive fissures within three rift zones (Fig. 11a; Ludden 1977; Lénat and Bachélery 1988; Lénat 1989. Eruption sites did not converge toward Dolomieu crater (1.2 km in diameter) or Bory crater (300 m in diameter) but oscillated inside the horseshoe-shaped caldera within approximately 5 km of the summit (Fig. 11b). Nine flank eruptions have occurred outside the caldera during the past 300 years (Stieltjes and Moutou 1989). Only fissure eruptions within the caldera occurred during the period 1842–1976. The central vent convergence time of Piton de la Fournaise is regarded as infinite, and the flank vent recurrence time, zero. The volcanic activity of the northwest rift zone is less frequent than those of the other rift zones. Figure 11c indicates that no eruptions occurred from sites with azimuths in the 270–360° range.

Model of intrusion sequence

A simple, idealized model is proposed to understand the uprift migration of eruption sites for a volcano with a throughgoing, well-developed rift zone. Time-series diagrams (Figs. 3–11) indicate that dikes are intruded into the upper crust including the volcanic edifice in systematic fashion as shown in Fig. 12a and b.

The direction of intrusion is governed by the local stress field, caused in part by previous dikes, and the regional stress field, based on the crack interaction theory proposed by Takada (1994a, b). In the idealized model, the stress field around a dike was estimated in Fig. 2 of Takada (1994a), and the stress relaxation with time around a dike was shown in Fig. 8. If the first dike is intruded beneath the left flank, the compressive stress around the first dike causes the second dike to intrude into the right flank. The third dike is emplaced within the left flank, because the compressive stress

Fig. 7 **a** Locality map of Fuji Volcano and **b, c** its r–t and θ–t diagrams. Positive values of distance from center are on the northwestern flank; negative values are on the southeastern flank. *Rectangle surrounded with dotted lines* represents positions where a major part of eruptions occurred. Other explanations are the same as in Fig. 3. Data compiled from Tsuya (1968), Miyaji (1988), and Uesugi (1993)

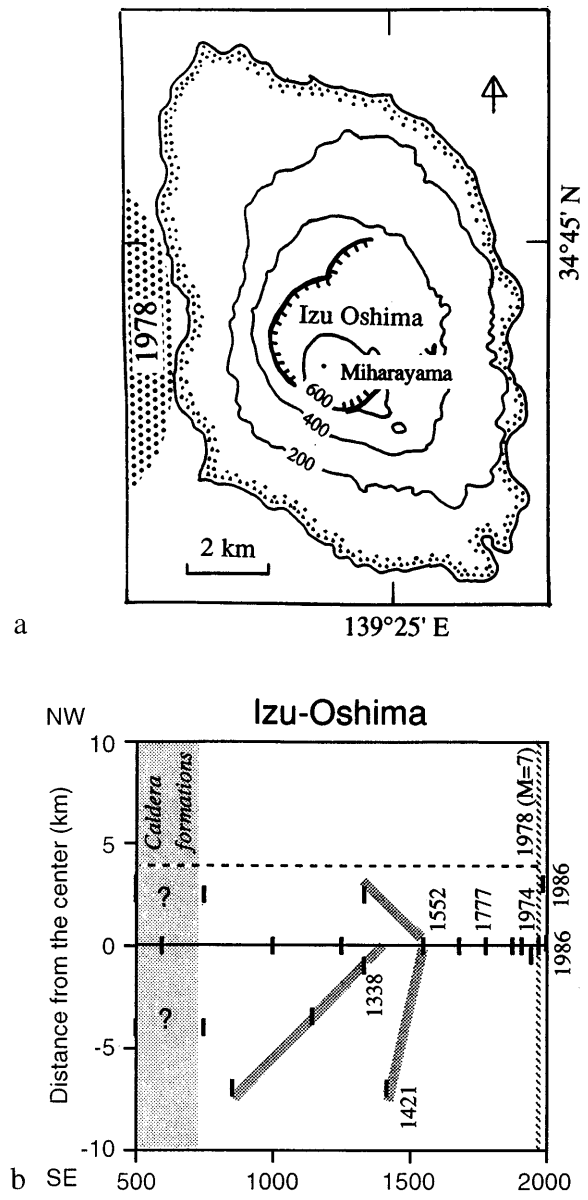

Fig. 8 **a** Locality map of Izu-Oshima Volcano and **b** its r–t diagram. *Stippled region* in **a** the foreshock area of the 1978 earthquake. Positive values of the distance from center are on the northwestern flank; negative are on the southeastern flank. *Horizontal dashed line* represents the northwestern limit of fissure eruption sites. *Vertical dotted line* large earthquake adjacent to the volcano. Other explanations are the same as in Fig. 3. Data compiled from Nakamura (1964), Tsumura et al. (1978), Isshiki (1984), and Sakaguchi et al. (1988)

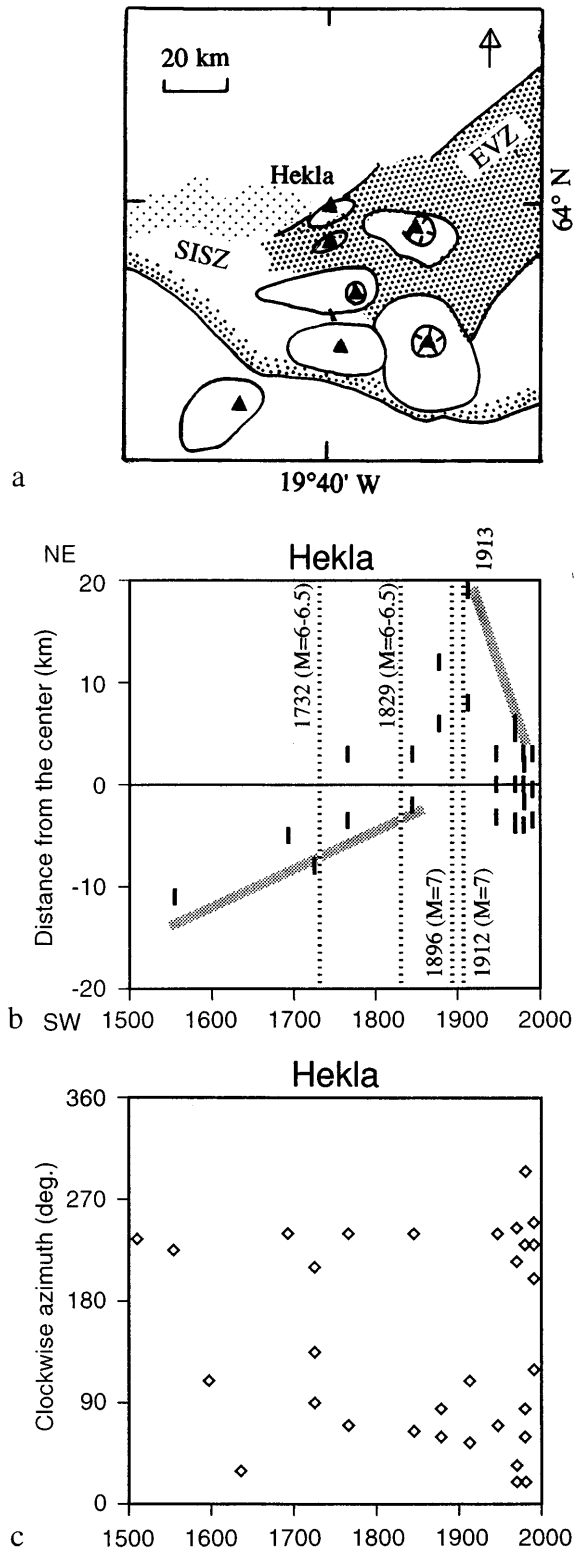

Fig. 9 **a** Locality map of Hekla Volcano and **b, c** its r–t and θ–t diagrams. *EVZ* East Volcanic zone; *SISZ* South Iceland Seismic zone; *solid triangle* the center of a central volcano. Positive values of distance from center are on the northeastern flank; negative values are on the southwestern flank. *Vertical dotted line* $M \geq 6$ earthquake adjacent to the volcanoes. Other explanations are the same as in Fig. 3. Data compiled from Thorarinsson (1967), Thorarinsson and Sigvaldason (1972), Gronvold et al. (1983), Einarsson (1986), and Gudmundsson et al. (1992)

from the first dike is more relaxed than that from the second dike. The intrusion, however, does not extend as far as the first dike, and it stops closer to the summit, because all the compressive stress is not relaxed. Even if a multiple dike occurs, the model is valid. The stress field produced by the second dike is superimposed on that from the first dike, unlike the case of a composite dike. The mechanical interaction of two cracks is preserved after the formation of a multiple dike. The

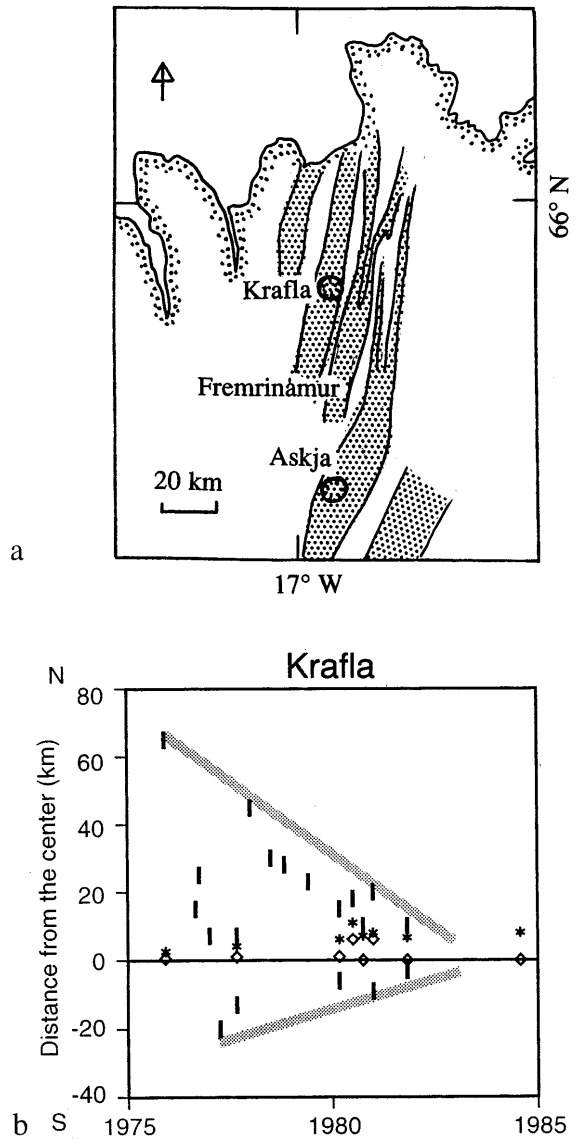

Fig. 10 **a** Locality map of Krafla Volcano and **b** its r–t diagram. *Stippled region* fissure swarms including volcanoes. Positive values of distance from center of Krafla caldera are on the northern flank; negative values are on the southern flank. *Asterisk* the northern termination of an eruptive fissure; *open diamond* the southern termination of an eruptive fissure. Other explanations are the same as in Fig. 3. Data compiled from Tryggvason (1984)

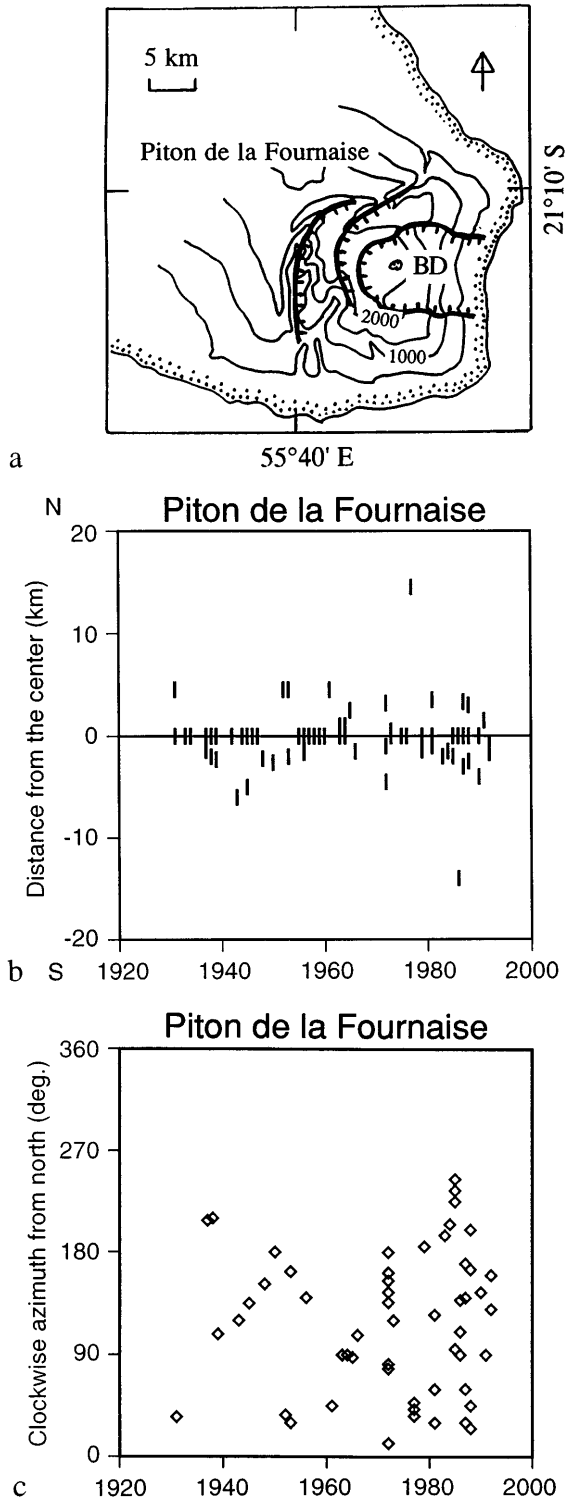

Fig. 11 **a** Locality map of Piton de la Fournaise Volcano and **b, c** its r–t and θ–t diagrams. Positive value of distance from center are on the northern flank; negative values are on the southern flank. *BD* Bory and Dolomieu craters. Other explanations are the same as in Fig. 3. Data compiled from Ludden (1977), Lénat and Bachélery (1988), Lénat (1989), Stieltjes and Moutou (1989), and Simkin and Siebert (1994)

fourth dike is emplaced within the right flank near the summit.

Due to the developing accumulation of dikes, the intrusion of the fifth dike is restricted to the area beneath the summit region, and a central eruption may be favored. If a long-lived vent through a weak zone, such as a central conduit, is formed, as suggested by thermal control (Bruce and Huppert 1990), central eruptions will tend to continue. Alternatively, near or during the central eruption phase, magma supply rates of some volcanoes at high levels may decrease, as suggested by the crustal deformation results of Ewart et al. (1990,

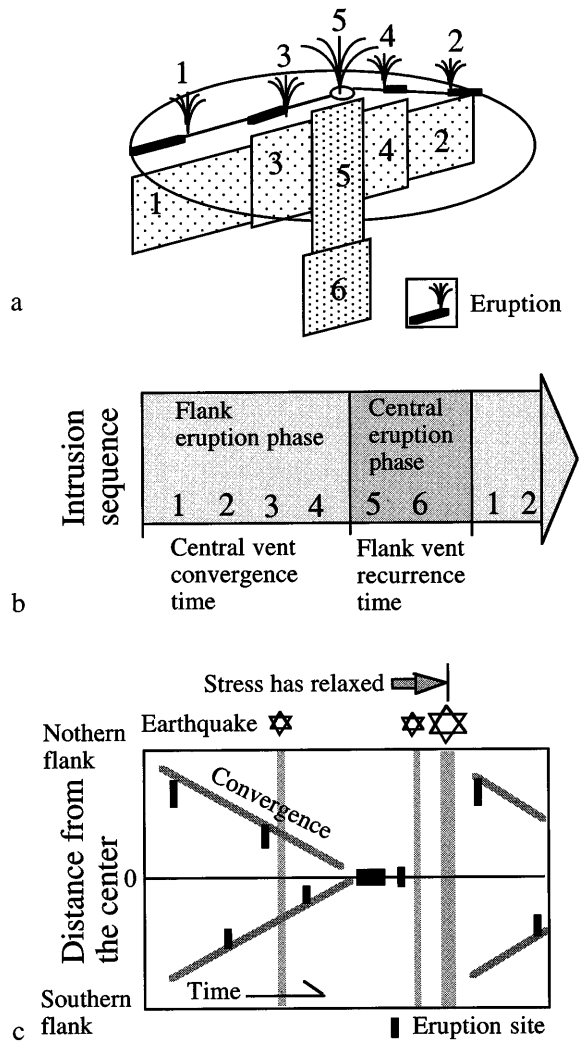

Fig. 12a–c Model of the intrusion sequence beneath a polygenetic volcano with cyclic activity. **a** A schematic subvolcanic structure with parallel dikes; **b** the intrusion sequence; **c** the time-series diagram of eruption sites (distance from center) of the volcano

1991). It may be interpreted that magma intrusion is suppressed to a deeper level to form the sixth dike, because of the accumulation of dike-induced stress in the volcanic edifice. Following dike emplacement, the volcano may become quiescent. If a central conduit is not closed, some intermittent eruptions may also occur. The local compressive stress increases with the accumulation of dikes during the central vent convergence time so that the upper crust, including the volcanic edifice, undergoes stress relaxation with brittle failure during the central eruption phase. Regional extension can also assist the relaxation process, as discussed below. After stress relaxation, the flank eruption phase recurs.

An ideal r–t diagram is shown in Fig. 12c on the assumption that the distance to the farthest fissure eruption site is proportional to the lateral extent of dike intrusion. Relating the fissure eruption sites to the intrusion distance is, however, somewhat problematic. We cannot know directly the orientation and dimensions of a dike intrusion in the shallow crust that includes the volcanic edifice. Intrusion records of Kilauea Volcano suggest that the distance between the center and the farthest down-rift eruptive fissure site is approximately related to the intrusion distance of the associated magma (Klein et al. 1987). Thus, the migration pattern of fissure eruption sites represents approximately that of dike intrusions including intrusion episodes (Kilauea type). On the other hand, eruption sites on Krafla Volcano were restricted within 11 km of the caldera center, unlike intrusion distances inferred from crustal deformation (Tryggvason 1984). In this case the migration pattern of fissure eruption sites does not represent that of dike intrusions (Krafla type; Fig. 10b). The intrusion sequence is applicable to both the Kilauea and Krafla types, but the migration pattern of eruption sites does not hold for the Krafla type.

There are some qualifications in applying the idealized model to a real case. In reality, the volcanoes that this paper treats have complicated magma plumbing systems. For example, the high-level magma plumbing system of Kilauea Volcano is comprised of a subcaldera magma reservoir, bilateral magma paths within the east rift zone, lateral dikes from the summit region, and a deep ultrabasic magma reservoir (Ryan et al. 1981; Ryan 1988). The convergence center of Krafla volcano shifted from the caldera center (Fig. 10b). Such a shift is, however, not a serious problem for this model, because a shift 10 km long is smaller than the northern extension 65 km long.

According to the model of intrusion sequence, intermittent central eruptions during the flank eruption phase are interpreted as a leak of magma through a central conduit. Some far-off flank eruptions during the central eruption phase are observed at Kilauea and Fuji volcanoes (Figs. 3c, 7b). If they originated from the sixth dike in Fig. 12a, they may avoid intruding into the more compressive flank near the summit by taking a roundabout way from below.

The intrusion sequence can apply to a dissected volcano with a dike swarm. The distribution-density of dikes decreases away from both sides of the volcano center (Walker 1987; Takada 1988). According to the intrusion sequence proposed in this paper, the dike number density decreases away from both sides of the center. The supposed, horizontal cross section of the left flank of Fig. 12a will reveal both the first and the third dikes around the center, and only the first dike away from the center. Additional dikes emplaced far from the center indicates a divergence of eruption sites. The number of distant dikes indicates the number of cycles of the flank eruption phase, if all the intrusions are associated with flank eruptions.

Boundary conditions governing the variation in cyclic activity

Regional stress and magma supply

The central vent convergence times and the flank vent recurrence times of the volcanoes in Table 1 are plotted on an "output-stress diagram" (Fig. 13) as proposed by Takada (1994c). Since the long-term volume ratio of magma output to input is estimated to be 0.1–0.3, using the ophiolite section or the seismic section of the oceanic crust, or the crustal deformation of an active volcano, the output-stress diagram can be inverted into the input-stress diagram with relative positions of volcanoes kept (Takada 1994c). The vertical axis is the crustal deformation (extension) rate; the horizontal axis is the average magma output rate, which may reflect the relative values of average magma supply. On a rift trend, a balance between the crustal deformation rate and the magma output rate is maintained.

For volcanoes plotted on or near a rift trend, the central vent convergence time is around 1–10 years, whereas the flank vent recurrence time is more than 100 years (Fig. 13; case 1 of Fig. 14). The condition that the regional differential stress is large favors the development of parallel dikes (Takada 1994a, b). Successive intrusions of parallel dikes cause a rapid increase in dike-induced stress in a direction parallel to the minimum principal regional compressive stress, so that they may shorten the central vent convergence time. More-

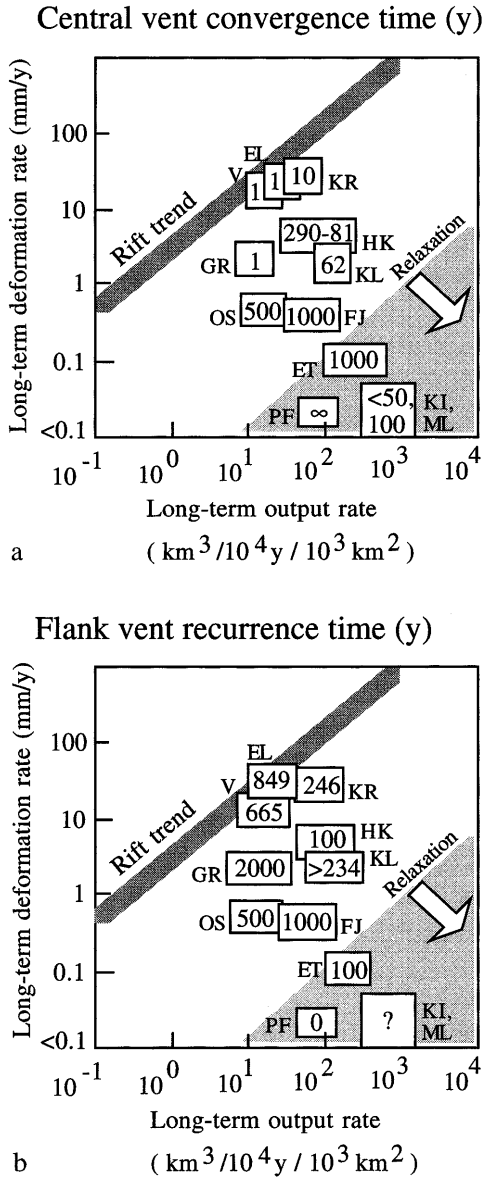

Fig. 13a, b Central vent convergence times and flank vent recurrence times plotted on the output-stress diagram defined by Takada (1994c). Data from Table 1, Khrenov et al. (1991; Kliuchevskoi Volcano), and Takada (1994c; the other volcanoes). *Numerals* represent central vent convergence times and flank vent recurrence times, respectively. *EL* Eldgjá-Lakagigar; *ET* Etna; *FJ* Fuji; *GR* Great rift; *HK* Hekla; *KI* Kilauea; *KL* Kliuchevskoi; *KR* Krafla; *ML* Mauna Loa; *OS* Izu-Oshima; *PF* Piton de la Fournaise; *V* Veidivötn

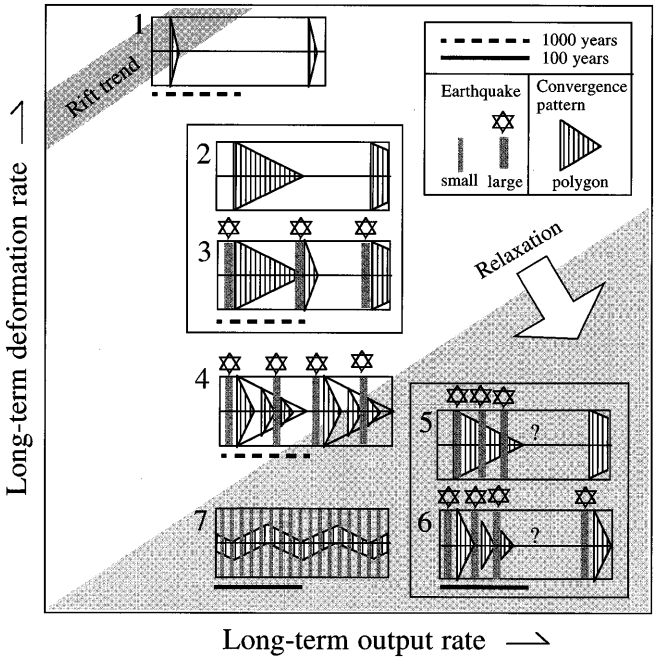

Fig. 14 Variation in the time-series diagram of eruption sites (distance from center) on the output-stress diagram depending on regional stress and magma supply. Near a rift trend, magma supply is suppressed during the central eruption phase. Far from a rift trend, the relaxation by faulting causes variation in the time-series diagrams. *1* The case without relaxation by faulting (the central vent convergence time (t_c) < the flank vent recurrence time (t_r); *2* the case without relaxation by faulting ($t_c \sim t_r$); *3* the case with relaxation by faulting ($t_c \sim t_r$); *4* the case showing a hierarchy structure with relaxation by faulting during the central eruption phase or near the second-order convergence points ($t_c > t_r$); *5* the case with relaxation by faulting during the flank eruption phase (short t_c and t_r); *6* the case showing a hierarchy structure with relaxation by faulting during the central eruption phase or near the second-order convergence points (short t_c and t_r); *7* the case showing an oscillation pattern of eruption sites with frequent seismicity of small magnitude

over, the central vent convergence time and the flank vent recurrence time of a monogenetic volcano field, as defined in Table 1, have tendencies similar to those of a polygenetic volcano (Fig. 13a). The average eruption interval of a monogenetic volcano field on a rift zone (e.g., Eldgjá-Lakagigar and Veidivötn, Iceland; Great rift, Idaho) is generally long (more than 500 years), but the average eruption volume is large.

For volcanoes plotted in the region far from a rift trend, the central vent convergence time increases, except for Hawaiian volcanoes, while the flank vent recurrence time decreases to less than 100 years. The condition that the regional differential stress is small favors the development of subparallel or radial dikes (Takada 1994a, b). Radial dikes emplaced in various directions slow down the increase in the dike-induced stress and delay the convergence of eruption sites. Moreover, the stress relaxation decreases stress concentration during the central vent convergence time, and shortens the flank vent recurrence time, as discussed below. Since Hawaiian volcanoes develop highly anisotropic rift zones, their convergence times may become of the order of 100 years.

Relaxation process

Regional spreading gradually releases the dike-induced compressive stress of those volcanoes near or on a rift trend. In the region near Krafla Volcano during the period of 1983–1985, the largest magnitude earthquake was $M \sim 5$ (Jacoby et al. 1989). Rift zones in Iceland develop numerous subparallel faults or open fissures (Forslund and Gudmundsson 1992), but a single large active fault has not been reported (Einarsson 1986). The dike-induced compressive stress may be released by the stress diffusion on the divergent plate boundary (Heki et al. 1993).

Exceptional rifts with large faults have, however, been reported; for example, East African rift (e.g., Dawson 1992) and Rio Grande rift (e.g., Chapin and Cather 1994). A rift valley bounded by normal faults develops in the following two cases: One case is when magma supply is not enough to compensate volumetrically for the regional crustal extension. For example, a rift valley is observed on the mid-ocean ridge at low spreading rates (Macdonald 1982). The low frequency of lateral dike intrusions along the spreading axis cannot totally cancel the sign of the stress induced by the regional extension. The other case is when magma ascent beneath a rift concentrates on a specific center such as a polygenetic volcano without lateral dikes.

Stress relaxation processes, which are defined as occurring within the contexts of both brittle and ductile behavior, play an important role in the growth of volcanoes plotted in the region far from a rift trend. Moreover, they may cause variation in the time-series diagrams. For example, in Hawaii, movements of normal faults parallel to rift zones relax the dike-induced, compressive stress accumulated at depth up to 5 km (e.g., Nakamura 1980; Dieterich 1988; Rubin 1990; Borgia et al. 1992; Borgia 1994; Takada 1994c). Movements of low-angle faults (décollement faults) at the base of the volcano relax the internal boundary loads applied by the compaction process within the 5- to 10-km-deep ultrabasic magma reservoir (Ryan 1988). However, the accumulation of dike-induced stress may trigger décollement faulting. But when is the compressive stress relaxed? The timing of brittle stress relaxation affects the pattern of the time-series diagram for eruption sites. Brittle stress relaxation during the flank eruption phase extends the central vent convergence time. Relaxation during the central eruption phase shortens the flank vent recurrence time.

Earthquakes that change the convergence pattern of eruption sites may need to disrupt an area almost equivalent to the cross section of a volcano or a sheeted-dike complex, i.e., of the order of 100–1000 km^2. Disrupted areas for $M = 6$ and $M = 7$ earthquakes are estimated approximately to be 130 km^2 and 1300 km^2, respectively (e.g., Utsu 1987). Thus, large earthquakes of magnitude ($M \geq 6$) should be identified with a convergence pattern.

The seismicity on the island of Hawaii was reported by Klein et al. (1987), Wyss and Koyanagi (1992), and Dvorak (1994). The major earthquakes were produced by décollement faults (e.g., Thurber and Gripp 1988; Arnadottir et al. 1991; Gillard et al. 1992; Wyss et al. 1992; Beisser et al. 1994). At Mauna Loa Volcano, earthquakes of $M \geq 6$ along or near the southwest rift zone (1868, $M = 7$, 7.9; 1887, $M = 6.5$; 1919, $M = 6.1$) and 40 km west or northwest of the volcano (1929, $M = 6.5$; 1950, $M = 6.4$; 1951, $M = 6.9$) occurred during the flank eruption phase. Moreover, large earthquakes also took place in Mauna Loa's southeast flank near or at the beginning of the central eruption phase (1962, $M = 6.1$; 1983, $M = 6.6$; Fig. 3b). At Kilauea Volcano, earthquakes of $M \geq 6$ occurred in the south flank just before the flank eruption phase or during the activity of a long-lived vent at a convergent point (1954, $M = 6.5$; 1975, $M = 7.2$; 1989, $M = 6.1$) (Fig. 3b). Thus, the timing of brittle stress relaxation may govern the difference in the convergence pattern between Mauna Loa (case 5 in Fig. 14) and Kilauea (case 6 in Fig. 14).

At Piton de la Fournaise Volcano, the general extensional deformation eastward (Lenat et al. 1989) acts along horseshoe-shaped faults (Fig. 11a; Duffield et al. 1982) during the flank eruption phase. The central vent convergence time of the volcano becomes infinite (case 7 in Fig. 14).

For volcanoes plotted at intermediate positions between the above two types, tectonic faulting may take part during stress relaxation (cases 3 and 4 in Fig. 14), while the volcano is spreading laterally through horseshoe-shaped faults or décollement-type faults (e.g., Figs. 5d, 11a; Borgia et al. 1992). It is difficult to classify historical earthquakes into tectonic earthquakes and those caused by the process of volcano edifice spread-

ing. In the region that includes Etna Volcano, large earthquakes occurred approximately 40 km south of the volcano in 1169 (M ~ 7) during the central eruption phase, and approximately 30 km southeast of the volcano in 1693 (M ~ 7) and approximately 70 km northeast of the volcano in 1908 (M = 7) at the second-order convergence point (Fig. 5a and b; Chester et al. 1985; Westaway 1992). At Izu-Oshima Volcano, the 1978 earthquake (M = 7) occurred during the central eruption phase, which resulted from tectonic strike-slip faulting west of the volcano (Fig. 8b; Tsumura et al. 1978). The foreshock area was within 10 km of the center of the volcano (Fig. 8a). At Hekla Volcano the volcanic activity near the convergence point or during the central eruption phase was affected by four earthquakes that occurred within 30 km west of the center of the volcano along SISZ (1732, M = 6–6.5, 20 km from the center; 1829, M = 6–6.5, 15–20 km; 1896, M = 7, 25 km; 1912, M = 7, 10 km; Fig. 9a and b; Einarsson 1986).

Adjacent local stress field

The asymmetric convergence of eruption sites (Figs. 1, 3–10) depends on circumference structures or the stress fields of adjacent volcanoes. Mauna Loa and Kilauea volcanoes are growing close to each other. Rift zones of the volcanoes extend asymmetrically (Figs. 3). The convergence point of Kilauea shifted downrift from Mauna Ulu to Pu'u O'o. Such asymmetric patterns of eruption sites, and the inverse correlations in volcanic activity (Stearns and Macdonald 1946; Moore 1971; Klein 1982), may have resulted from magma-induced mechanical interactions between volcanoes (Takada 1994d). At Kliuchevskoi Volcano, the asymmetric distribution of eruption sites suggests that the volcano is affected mechanically by the adjacent volcanoes within 10 km of the volcano (Kamen, Bezymianny, and volcanoes from west to northwest of the volcano; Fig. 4a). At Sakurajima Volcano the asymmetric pattern of eruption sites and the irregular rotation of eruption sites may have resulted from the unrelaxed stress of the older volcano, Kitadake, 2 km north of the Minamidake cone (Figs. 6a–d). At Krafla Volcano dike intrusions beneath the southern flank may have been interacting mechanically with northerly intrusions from Askja Volcano (Fig. 10a; Ryan 1990). The stress diffusion model of Heki et al. (1993) indicates that the eruption interval of approximately 100 years is enough to relax the stress for mechanical interaction. However, the geometric evidence that two rift zones of these volcanoes are almost overlapping supports mechanical interaction.

Evolution of a volcano with complexity

Time-series diagrams of eruption sites can provide information on the near-future conditions and on the evolution of a volcano during periods of 10–1000 years if one assumes both a constant supply rate of magma and constant regional stress. The foregoing sections discussed the intrusion sequence and the variation of the convergence pattern of eruption sites mainly by crack interaction through accumulated, dike-induced stress and its relaxation, i.e., by self-control of the magma plumbing system at constant boundary conditions.

However, some time-series diagrams show very complicated migration patterns of eruption sites. For example, eruption sites at Piton de la Fournaise do not converge but oscillate or fluctuate. Some volcanoes exhibit an apparent hierarchy of convergence. The boundary conditions may fluctuate. The magma plumbing system may respond well to a change in boundary conditions. An abrupt divergence of eruption sites near the convergence point (Figs. 6a, 8b) may be caused by magma supply of large volume or an abrupt change in the regional stress field (case 3 in Fig. 14). It is difficult to obtain the relevant data indicating the changes in the previous boundary conditions that correspond with a complicated time-series diagram.

This paper has conveniently defined the flank eruption phase and the central eruption phase by the frequency of flank eruptions or central eruptions without flank eruptions. However, we cannot easily distinguish the central eruption phase from the flank eruption phase at some volcanoes. Partitioning of magma within a volcano may be useful to clarify the alternation between the two phases. The period that a large proportion of supplied magma moved beneath the flank of a volcano, e.g., 1968–1984 at Mauna Loa (Peterson and Moore 1987), 1932–1993 at Kluichevskoi (Khrenov et al. 1991; Ozerov et al. 1994), and 1200–1994 at Etna (Chester et al. 1985; Simkin and Siebert 1994), may be equivalent to the flank eruption phase proposed in this paper. The period that a large proportion of supplied magma erupted through a central conduit, e.g., the period since 1955 at Sakurajima (Kobayashi 1988), and 3000–2000 years BP at Fuji (Miyaji 1988), may be equivalent to the central eruption phase proposed in this paper. Thus, a distinctive episode of summit activity that marks the termination of flank vent convergence may be the first central eruption with a large eruption volume of magma or a continuous eruption at a constant high eruption rate after the convergence. Volume partitioning of magma will have to be discussed with migration patterns of eruption sites.

With regard to the evolution of polygenetic volcanoes, several problems must be addressed. During the cyclic activity of a polygenetic volcano, the collapse of the volcano, such as by caldera formation or by failure of an unstable flank, may occur. In particular, the compressive stress increases with accumulation of dike intrusions within the volcano during the flank eruption phase, whereas the slope of the flank increases with volcano growth during the central eruption phase. These instabilities should be accounted for. Next, during the period of volcano growth, the accumulation of dike intrusions may cause a shift in the main magma

path or vent, such as the shift of a long-lived vent at Kilauea. Since a polygenetic volcano is evolving mechanically, thermally, and chemically, the cycle of a constant interval may not be expected in the long-term. This paper discusses only the mechanical evolution of the volcano. The thermal evolution will also have to be considered and integrated with the mechanical model in order to construct the most plausible model for volcano evolution.

Conclusions

Fissure eruption sites of some volcanoes migrated toward the center (the summit, the caldera, or the central vent; Mauna Loa, Kilauea, Kliuchevskoi, Etna, Sakurajima, Fuji, Izu-Oshima, and Hekla volcanoes). Only terminations of dikes migrated toward the center at Krafla Volcano. There is variation in the convergence pattern of eruption sites: a hierarchy of first-order and second-order convergences, asymmetric convergence and the abrupt divergence of eruption sites. After the convergence of eruption sites, the central eruption phase is attained. Eruption sites of Piton de la Fournaise Volcano did not converge but oscillated around the center.

Based on the time-series diagram of eruption sites or intrusion distances, an ideal intrusion sequence, as shown in Fig. 13, is proposed at a constant magma supply under constant regional stress.

Variations in the time-series diagram are governed by regional stress and magma supply. Under the condition that the balance of the regional extension and the magma supply is maintained (near or on a rift trend as defined by Takada 1994c), the central vent convergence time during the flank eruption phase becomes 1–10 years, whereas the flank vent recurrence time during the central eruption phase extends to more than 100 years due to a decrease in magma supply. Under the condition that the magma supply prevails over the regional extension (far from a rift trend), the central vent convergence time lengthens, whereas the flank vent recurrence time shortens owing to stress relaxation due to faulting. The stress relaxation process plays an important role in the variation and hierarchy of convergence patterns observed. Asymmetric convergence is caused by an adjacent, local stress field such as volcano–volcano interaction.

Acknowledgements I greatly benefited from constructive reviews by E. W. Wolfe, M. P. Ryan, A. Gudmundsson, and W. Hildreth. I thank C. Mandeville for valuable comments and critical reading of this manuscript. Discussions with M. Takahashi, N. Miyaji, and Y. Kawanabe at an early stage of this work were very helpful.

References

Arnadottir T, Segall P, Delaney P (1991) A fault model for the 1989 Kilauea south flank earthquake from leveling and seismic data. Geophys Res Lett 18:2217–2220

Beisser M, Gillard D, Wyss M (1994) Inversion for source parameters from sparse data sets: test of the method and application to the 1951 (M=6.9) Kona, Hawaii, earthquake. J Geophys Res 99:19661–19678

Borgia A (1994) Dynamic basis of volcanic spreading. J Geophys Res 99:17791-17804

Borgia A, Ferrari L, Pasquaré G (1992) Importance of gravitational spreading in the tectonic and volcanic evolution of Mount Etna. Nature 357:231–235

Brandsdóttir B, Einarsson P (1979) Seismic activity associated with the September 1977 deflation of the Krafla central volcano in northeastern Iceland. J Volcanol Geotherm Res 6:197–212

Bruce PM, Huppert HE (1990) Solidification and melting along dykes by the laminar flow of basaltic magma. In: Ryan MP (ed) Magma transport and storage. Wiley, Chichester, pp 87–101

Chapin CE, Cather SM (1994) Tectonic setting of the axial basins of the northern and central Rio Grande rift. In: Keller GR, Cather SM (eds) Basins of the Rio Grande rift: structure, stratigraphy, and tectonic setting. Geol Soc Am Spec Pap 291:1–25

Chester DK, Duncan AM, Guest JE, Kilburn CRJ (1985) Mount Etna: the anatomy of a volcano. Chapman and Hall, London, pp 1–404

Dawson JB (1992) Neogene tectonics and volcanicity in the North Tanzania sector of the Gregory Rift Valley: contrasts with the Kenya sector. Tectonophysics 204:81–92

Dieterich JH (1988) Growth and persistence of Hawaiian volcanic rift zones. J Geophys Res 93:4258–4270

Duffield WA, Stieltjes L, Varet J (1982) Huge landslide blocks in the growth of Piton de la Fournaise, La Réunion, and Kilauea volcano, Hawaii. J Volcanol Geotherm Res 12:147–160

Dvorak J (1994) An earthquake cycle along the south flank of Kilauea volcano, Hawaii. J Geophys Res 99:9533–9541

Einarsson P (1986) Seismicity along the eastern margin of the North American Plate. In: Vogt PR, Tucholke BE (eds) The geology of North America, vol M. The western North Atlantic region. Geological Society of America, Boulder, Colorado, pp 99–116

Einarsson P (1991) Earthquakes and present-day tectonism in Iceland. Tectonophysics 189:261–279

Ewart JA, Voight B, Björnsson A (1990) Dynamics of Krafla caldera, north Iceland:1975–1985. In: Ryan MP (ed) Magma transport and storage. Wiley, Chichester, pp 225–276

Ewart JA, Voight B, Björnsson A (1991) Elastic deformation models of Krafla volcano, Iceland, for the decade 1975 through 1985. Bull Volcanol 53:436–459

Forslund T, Gudmundsson A (1992) Structure of Tertiary and Pleistocene normal faults in Iceland. Tectonics 11:57–68

Gillard D, Wyss M, Nakata JS (1992) A seismotectonic model for western Hawaii based on stress tensor inversion from fault plane solutions. J Geophys Res 97:6629–6641

Gronvold K, Larsen G, Einarsson P, Thorarinsson S, Saemundsson K (1983) The Hekla eruption 1980–1981. Bull Volcanol 46:349–363

Gudmundsson A, Oskarsson N, Gronvold K, Seamundsson K, Sigurdsson O, Stefansson R, Gislason SR, Einarsson P, Brandsdóttir B, Larsen G, Johannesson H, Thordarson T (1992) The 1991 eruption of Hekla, Iceland. Bull Volcanol 54:238–246

Heki K, Foulger GR, Julian BR, Jahn C-H (1993) Plate dynamics near divergent boundaries: geophysical implications of postrifting crustal deformation in NE Iceland. J Geophys Res 98:14279–14297

Holcomb RT (1987) Eruptive history and long-term behavior of Kilauea Volcano. In: Decker RW, Wright TL, Stauffer P (eds) Volcanism in Hawaii. US Geol Surv Prof Pap 1350:261–350

Isshiki N (1984) Explanatory text and the geologic map of Japan (scale 1:50000), O Shima. Geological Survey of Japan (in Japanese with English abstract)
Jacoby WR, Zdarsky H, Altmann U (1989) Geodetic and geophysical evidence for magma movement and dyke injection during the Krafla rifting episode in North Iceland. Geophys Monogr 57:65–77
Khrenov AP, Dvigalo VN, Kirsanov IT, Fedotov SA, Gorel'chik VI, Zharinov NA (1991) Klyuchevskoy volcano. In: Fedotov SA, Masurenkov YP (eds) Active volcanoes of Kamchatka, vol. 1. Nauka Publishers, Moscow, pp 106–153
Klein F W (1982) Pattern of historical eruptions at Hawaiian volcanoes. J Volcanol Geotherm Res 12:1–35
Klein FW, Koyanagi RY, Nakata JS, Tanigawa WR (1987) The seismicity of Kilauea's magma system. In: Decker RW, Wright TL, Stauffer P (eds) Volcanism in Hawaii. US Geol Surv Prof Pap 1350:1019–1185
Kobayashi T (1988) Geology and petrology. In: Aramaki S, Kamo K, Kamada M (eds) A guide book for Sakurajima volcano. Organizing committee, Kagoshima international conference on volcanoes, pp 12–27
Kobayashi T, Ishihara K (1988) Historic eruptions and Recent activities. In: Aramaki S, Kamo K, Kamada M (eds) A guide book for Sakurajima volcano. Organizing committee, Kagoshima international conference on volcanoes, pp 7–11
Koide H, Bhattacharji S (1975) Mechanism interpretation of rift valley formation. Science 189:791–793
Kuntz MA, Champion DE, Spiker EC, Lefebvre RH (1986) Contrasting magma types and steady-state, volume-predictable, basaltic volcanism along the Great rift, Idaho. Geol Soc Am Bull 97:579–594
Larsen G (1984) Recent volcanic history of the Veidivötn fissure swarm, southern Iceland: an approach to volcanic risk assessment. J Volcanol Geotherm Res 22:33–58
Lénat JF, Bachélery P (1988) Dynamics of magma transfer at Piton de la Fournaise volcano (Réunion Island, Indian Ocean). In: Chi-Yu, Scarpa R (eds) Modeling of magmatic process. Earth Evolution Science Special Issue, Friedrich Vieweg and Sohn, Braunschweig/Wiesbaden, pp 57–72
Lénat JF, Bachélery P, Bonneville A, Hirn A (1989) The beginning of the 1985–1987 eruptive cycle at Piton de la Fournaise (La Réunion); new insights in the magmatic and volcano-tectonic system. J Volcanol Geotherm Res 36:209–232
Lipman P (1980a) The southwest rift zone of Mauna Loa: implications for structural evolution of Hawaiian volcanoes. Am J Sci 280A:752–776
Lipman P (1980b) Rates of volcanic activity along the southwest rift zone of Mauna Loa volcano, Hawaii. Bull Volcanol 43:703–725
Lockwood JP (1995) Mauna Loa history: the preliminary radiocarbon record. In: Rhodes JM, Lockwood JP (eds) Mauna Loa revealed. Geophys Monogr 92:81–94
Lockwood J, Lipman P (1987) Holocene eruptive history of Mauna Loa volcano. US Geol Surv Prof Pap 1350:509–535
Lockwood J, Dvorak J, English T, Koyanagi R, Okamura A, Summers M, Tanigawa W (1987) Mauna Loa 1974–1984: a decade of intrusive and extrusive activity. US Geol Surv Prof Pap 1350:537–570
Ludden JN (1977) Eruptive patterns for the volcano Piton de la Fournaise, Reunion Island. J Volcanol Geotherm Res 2:385–395
Macdonald KC (1982) Mid-ocean ridges: fine-scale tectonic, volcanic and hydrothermal processes within the plate boundary zone. Ann Rev Earth Sci 10:155–190
Macdonald GA, Abbott AT, Peterson FL (1983) Volcanoes in the sea. University of Hawaii Press, Honolulu, pp 1–517
Miyaji N (1988) History of younger Fuji volcano. J Geol Soc Jpn 94:433–452 (in Japanese with English abstract)
Moore J G (1971) Relationship between subsidence and volcanic load, Hawaii. Bull Volcanol 34:562–576
Nakamura K (1964) Volcano-stratigraphic studies of Oshima Volcano, Izu. Bull Earthquake Res Inst Univ Tokyo 42:649–728
Nakamura K (1980) Why do long rift zones develop in Hawaiian volcanoes? A possible role of thick oceanic sediments. Bull Volcanol Soc Jpn 25: 255–269 (in Japanese with English abstract)
Ozerov A, Taran Y, Sato K (1994) The 1994 eruption of Klyuchevskoy. Chishitsu News, Geological Survey of Japan 484:69 (in Japanese)
Peterson DW, Moore RB (1987) Geologic history and evolution of geologic concepts, Island of Hawaii. In: Decker RW, Wright TL, Stauffer P (eds) Volcanism in Hawaii. US Geol Surv Prof Pap 1350:149–189
Romano R (1991) Mt. Etna, Naturalistic and touristic map, scale 1:60000. Sociatá elaborazioni cartografiche, Firenze
Rubin AM (1990) A comparison of rift-zone tectonics in Iceland and Hawaii. Bull Volcanol 52:302–319
Rubin AM, Pollard DD (1988) Dike-induced faulting in rift zones of Iceland and Afar. Geology 16:413–417
Ryan MP (1988) The mechanics and three-dimensional internal structure of active magmatic systems: Kilauea volcano, Hawaii. J Geophys Res 93:4213–4248
Ryan MP (1990) The physical nature of the Icelandic magma transport system. In: Ryan MP (ed) Magma transport and storage. Wiley, Chichester, pp 175–224
Ryan MP, Koyanagi RY, Fiske RS (1981) Modeling the three-dimensional structure of macroscopic magma transport systems: application to Kilauea volcano, Hawaii. J Geophys Res 86:7111–7129
Sakaguchi K, Takada A, Uto K, Soya T (1988) The 1986 eruption and products of Izu-Oshima volcano, Japan. Bull Volcanol Soc Jpn Spec 33: S20-S31 (in Japanese with English abstract)
Simkin T, Siebert L (1994) Volcanoes of the world, 2nd edn. Geoscience Press, Tucson, pp 1-349
Stearns HT, Macdonald GA (1946) Geology and ground water resources of the Island of Hawaii. Hawaii Div Hydrogr Bull 9:1–363
Stieltjes L, Moutou P (1989) A statistical and probabilistic study of the historic activity of Piton de la Fournaise, Réunion Island, Indian Ocean. J Volcanol Geotherm Res 36:67–86
Stieltjes L, Bachelery P, Bacquet A, Villéle A de, Kasser M, Lénat JF, Moutou P (1986) Carte des Coulees Historiques du Volcan de la Fournaise, 1:25000. Bureau de Recherches Géologiques et Miniéres
Takada A (1988) Subvolcanic structure of the central dike swarm associated with the ring complexes in the Shitara district, central Japan. Bull Volcanol 50:106–118
Takada A (1994a) Development of a subvolcanic structure by the interaction of liquid-filled cracks. J Volcanol Geotherm Res 61:207–224
Takada A (1994b) Accumulation of magma in space and time by crack interaction. In: Ryan MP (ed) Magmatic systems. Academic Press, San Diego, Calif, pp 241–257
Takada A (1994c) The influence of regional stress and magmatic input on styles of monogenetic and polygenetic volcanism. J Geophys Res 99:13563–13573
Takada A (1994d) Mechanical interaction between volcanoes. IAVCEI Ankara 1994 abstracts
Thorarinsson S (1967) The eruption of Hekla 1947–1948. I. The eruption of Hekla in historical times. Soc Scientiarum Islandica, Reykjavik, pp 1–170
Thorarinsson S, Sigvaldason GE (1972) The Hekla eruption of 1970. Bull Volcanol 36:1–20
Thordarson Th, Self S (1993) The Laki (Skaftár fire) and Grímsvötn eruptions in 1783–1785. Bull Volcanol 55:233–263
Thurber CH, Gripp AE (1988) Flexure and seismicity beneath the south flank of Kilauea volcano and tectonic implications. J Geophys Res 93:4271–4278
Tryggvason E (1984) Widening of the Krafla fissure swarm during the 1975–1981 volcano-tectonic episode. Bull Volcanol 47:47–69

Tsumura K, Karakama I, Ogino I, Takahashi M (1978) Seismic activities before and after the Izu-Oshima-kinkai earthquakes of 1978. Bull Earthquake Res Inst Univ Tokyo 53:675–706 (in Japanese with English abstract)

Tsuya (1968) Geology of volcano Mt. Fuji. Explanatory text of geologic map 1:50000 scale. Geological Survey of Japan

Uesugi Y (1993) Tephrostratigraphic eruption forecasts of Fuji volcano, Central Japan. Quaternary Res 32:271–282 (in Japanese)

Utsu T (1987) Standard relations between shallow earthquakes and fault parameters. In: Utsu T, Shima E, Yoshii T, Yamashina K (eds) Encyclopedia of earthquake. Asakura, Tokyo, pp 243–244 (in Japanese)

Walker GPL (1987) The dike complex of Koolau volcano, Oahu: internal structure of a Hawaiian rift zone. US Geol Surv Prof Pap 1350:961–993

Westaway R (1992) Seismic moment summation for historical earthquakes in Italy: tectonic implications. J Geophys Res 97:15437–15464

Wyss M, Koyanagi R (1992) Isoseismal maps, macroseismic epicenters, and estimated magnitudes of historical earthquakes in the Hawaiian islands. US Geol Surv Bull 2006:1–93

Wyss M, Liang B, Tanigawa WR, Wu X (1992) Comparison of orientations of stress and strain tensors based on fault plane solutions in Kaoiki, Hawaii. J Geophys Res 97:4769–4790